# A shortcut for determining growth mode*

R. A. Rehman[a)b)†], Cai Yi-Liang(蔡亦良)[a)], Zhang Han-Jie(张寒洁)[a)], Wu Ke(吴 珂)[a)], Dou Wei-Dong(窦卫东)[a)], Li Hai-Yang(李海洋)[a)], He Pi-Mo(何丕模)[a)], and Bao Shi-Ning(鲍世宁)[a)]

[a)] *Physics Department, Zhejiang University, Hangzhou* 310027, *China*
[b)] *Physics Department, Forman Christian College University, Lahore* 54600, *Pakistan*

(Received 7 February 2013; revised manuscript received 26 April 2013)

Thin and thick films of iron phthalocyanine (FePc) molecules are deposited on a Ag (110) surface. The nature of the FePc growth and the interaction with the substrate have been studied by X-ray photoelectron spectroscopy (XPS). All of the core level spectra exhibit rigid shifts towards lower binding energies following the deposition of the organic films, each by a different magnitude. A greater change and a larger shift in the Fe2p level as compared to C1s core level reveals that the adsorbate interacts with the substrate mainly via the Fe atom, located at the center of the molecule. An increase/decrease in the intensity of C1s/Ag3d level is found to be exponentially linked to the overlayer molecular coverage. Finally, the so-called growth/decay curve indicates that FePc thin films initially develop following the FM growth mode and then transform to SK mode, resulting in 3D island aggregation.

**Keywords:** iron phthalocyanine, silver, growth modes, X-ray photoelectron spectroscopy

**PACS:** 72.80.Le, 34.20.Gj, 34.35.+a, 42.70.Jk **DOI:** 10.1088/1674-1056/22/10/107202

## 1. Introduction

In order to extend the enormous amounts of knowledge for the metal phthalocyanine (MPc) molecules, a lot of research has been done in the past quarter century. Such organic semiconductors are well suited to applications in the fields of fuel cells,[1] gas sensors (especially for the detection of $NO_2$),[2] magnetic switches,[3] and organic spintronics devices.[4] Most recently, zinc-substituted phthalocyanine (ZnPc) has been revealed as a promising candidate for photodynamic cancer therapy.[5] Iron and cobalt phthalocyanine (FePc, CoPc) semiconductors have been considered promising materials in the development of low dimensional molecular magnets.[6,7]

The functionality of these organic molecules can be tuned; however, small modifications of the molecule can significantly change the electronic properties.[8] Since MPcs can be applied in variety of devices and their properties can be tuned, the degree of molecular ordering at an interface and a detailed understanding of the interface formation and its electronic properties that are crucial in improving the efficiency of molecular-based devices are of utmost importance. Due to the wide spectrum of applications and unique properties of phthalocyanines (Pc), several groups around the globe have either been interested in unsubstituted phthalocyanine, abbreviated $H_2Pc$,[9] MPc.[6,7] Generally, Pc is a macrocyclic compound which consists of four isoindole-class $[(C_6\ H_4)\ C_2N]$ units linked by four nitrogen atoms to form a conjugated chain and which can host various different metal ions in its center. Like ZnPc and CoPc, an FePc molecule also has a planar structure with $D_{4h}$ point symmetry.

An FePc molecule consists of a central Fe atom surrounded by four pyrrole nitrogen ($N_{pyr}$), four-bridging aza nitrogen ($N_{b.aza}$), eight-pyrrole carbon ($C_{pyr}$), and 24-benzene ring carbon ($C_{benz}$). Among the MPcs, the FePc molecule has been widely studied. For example, Fortuna *et al.* and Betti *et al.* have studied FePc on highly pyrolitic graphite (HOPG),[10] Ag (110),[11] and Au (110) surfaces,[12,13] respectively. FePc on a Ag (110) surface has also been studied by Palmgren *et al.*[14] who found temperature-dependent ordering at the sample surface. The same molecule has also been studied on Ag (111) with a focus on commensurate ordering and structural and electronic properties at the interface.[15,16]

Recently, the electronic properties of FePc on Ag (110) have been investigated by valence level photoemission spectroscopy (VL-PES) and the findings were explained in the framework of density functional theory (DFT) calculations.[17] Since the transition FePc on Ag (110) substrate has already been repeatedly studied by means of photoemission spectroscopy (PES) and scanning tunneling microcopy (STM), another study on this system seems to be a waste of time. However, two fundamental issues which unfortunately have been missing in almost all the above-mentioned FePc related studies are: i) the proper molecular coverage estimation, and ii) the molecular growth mode determination. This deficiency makes it difficult to fully understand the adsorption of FePc on metal substrate. Also, it is well known that the charge transfer efficiency, which in fact depends on the molecular orienta-

*Project supported by the National Natural Science Foundation of China (Grants Nos. 10974172, 10774129, and 61106131) and the Fundamental Research Funds for the Central Universities.
†Corresponding author. E-mail: ateeq215@gmail.com
© 2013 Chinese Physical Society and IOP Publishing Ltd 

tion, greatly influences the performance of organic electronic devices.[18] Therefore, we decided to carry out the photoemission study of FePc on twofold silver substrate with the highest aims for proper background subtraction procedure, proper coverage determination, and epitaxial growth mode investigation. The growth modes for the mono- and multilayer of FePc on Ag (110) are revealed by means of core level-photoemission spectroscopy (CL-PES) or equivalently called electron spectroscopy for chemical analysis (ESCA). The present study in conjunction with the previously established findings thus may provide a complete set of information necessary to fully understand the fundamental issues regarding the overlayer-substrate interaction and growth mode determination.

## 2. Experimental

All the experiments were performed with a VG ESCALAB MARK II surface analysis system. In brief, the system is composed of two inter-connected ultra-high vacuum (UHV) chambers: the preparation chamber and the analysis chamber. The former is used to prepare the samples and the latter is used to analyze the samples. Conceptually, a metallic dome at the top of the instrument is the electron spectrometer (hemispherical analyzer) which is connected to the analysis chamber below it by a long tube containing the electron lenses and apertures. The analysis chamber and housing for the hemispherical analyzer are formed from mu-metal (77% Ni, 15% Fe, plus Cu and Mo), an alloy which screens out external magnetic fields. A stainless steel preparation chamber is connected right to the analysis chamber and equipped with a Ta boat evaporator and an argon ion sputter gun. Each chamber houses a rotating arm on a translational mechanism that is used to any of the ports and stations on the preparation and analysis chamber. In contrast to the preparation chamber, the sample stages in the analysis chamber can be moved in all three spatial directions and can be rotated around its axis.

Additionally, each chamber allows parking of two sample carrying buses, and each bus can accommodate a maximum of six samples. Furthermore, in the former chamber, samples can be annealed either by indirect heating or, for semiconductor samples, by direct heating. The latter chamber is equipped with a twin-anode X-ray gun (monochromatic Al $K_\alpha = 1486.6$ eV and unmonochromatic Mg $K_\alpha = 1253.56$ eV) and a hemispherical analyzer. The respective line widths of Al $K_\alpha$ and Mg $K_\alpha$ are 0.85 eV and 0.75 eV.[19] While knowing the fact that Mg anode produces a narrower $K_\alpha$ line than the Al, the latter anode was used since it offers higher intensity as compared to the Mg anode. Additionally, the base pressure in both chambers was in the $2 \times 10^{-10}$ mbar (1 bar = $10^5$ Pa) range, which helps to minimize contamination during sample preparation and analysis. In addition, the system is also equipped with a resistive-heating tantalum (Ta) boat evaporator. As a substrate, we used a low index (110) silver single crystal. The *ex situ* cleaning was done ultra-sonically.

For *in situ* cleaning, the samples were mounted on vertically fixed Mo sample holders where the samples were cleaned by the standard repeated cycles of 1-keV $Ar^+$ sputtering and annealing at 810 K. The surface quality and cleanliness of the samples were checked by X-ray photoelectron spectroscopy (XPS or CL-PES). After the treatment no oxygen or carbon traces were detected. A few mg of dark blue colored FePc powder purchased from Sigma Aldrich Co. Ltd was used as an adsorbate. Prior to the sample preparation, the adsorbate was purified by long-time degassing at a temperature slightly lower than the sublimation temperature. The organic thin–thick films were then deposited from a resistively heated Ta boat at an evaporation temperature of about 540 K on the Ag (110) surface. During deposition, the Ag substrate was kept at room temperature in order to prevent dissociation of the molecules after deposition. The incident and emission angles, respectively, were 30° and 78°. All the measurements were performed in the constant energy mode. The pass energies were 50 eV and 25 eV for wide and narrow scans and the scanning steps were 0.5 eV and 0.2 eV, respectively. During the experiments, the operating conditions for the incident radiation were 15 kV and 20 mA. A high resolution and background-subtracted survey spectrum of bare Ag (110) surface integrated over 1–10 scans is displayed in Fig. 1. The deposition rate as estimated from the XPS intensity ratios of the overlayer and substrate signals, using a well-developed method,[20] is $\approx 1.43$ Å/min, and is illustrated in detail in the following section. The instrument was calibrated with pure gold and copper standard samples by setting energies of $(83.97 \pm 0.02)$ eV and $(932 \pm 0.02)$ eV, respectively. Spectral analysis was carried out using the standard CasaXPS software. In all experimental results, thicknesses are reported in angstroms (Å).

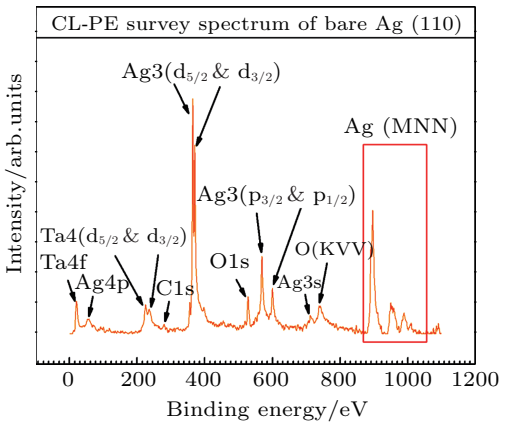



**Fig. 1.** (color online) A typical core level photo-emission (CL–PE) survey spectrum of an untreated Ag (110) surface, showing the peaks of the individual elemental orbitals.

## 3. Results and discussion

A background-subtracted typical CL-PE survey spectrum of bare Ag (110) surface is shown in Fig. 1, where many peaks originating from individual elemental orbitals are clearly seen. The spectrum is dominated by five Ag CL emissions (3($d_{5/2}$, $d_{3/2}$, $p_{3/2}$, $p_{1/2}$), 3s) and the Ag (MNN) Auger peak located at binding energies of 363.72, 370.77, 567.43, 599.86, 739.53, and 898.02 eV, respectively. Besides oxygen (527.96 eV), a weak peak of Ta is also found. Non metal (C: carbon, 281.25 eV) is also detected owing to the presence of adsorbed hydrocarbons. Perhaps the small amount of C1s and O1s emissions results from the *ex situ* preparation process or the transfer process of the sample into the UHV chamber. The intense transition metal peak in the survey spectrum originates from the Ta resistive-heating boat upon which the sample was mounted. Each major and minor peak has been marked for the assistance of the reader. The argon ion-treated samples did not reveal any contamination, which verifies the cleanliness of the samples. A large background generated by the inelastic scattering of photoelectrons is always expected in the spectra obtained by surface sensitive photoexcited techniques. Therefore, in order to get background-free data we considered all the background types — namely the Shirley, the linear, and the Touggard, which are illustrated in the upper part of both the panels in Fig. 2.

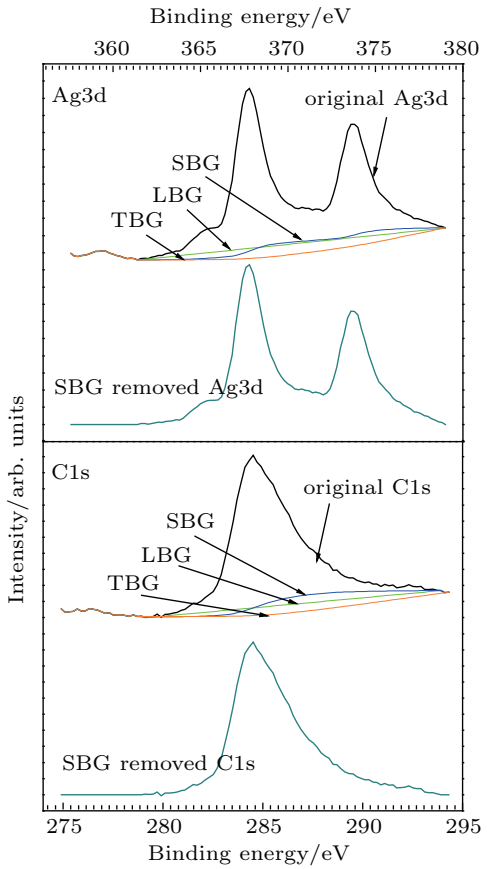



**Fig. 2.** (color online) Thick spectra of Ag3d (upper panel) and C1s (lower panel) showing the background removal procedure. For simplicity, all three background types are shown: Shirley (S), linear (L), Touggard (T). It is clear from the figure that only a Shirley type background fits nicely to the Ag3d and C1s spectra.

Figure 2 clearly demonstrates that among all the three well-known background types, only the Shirley-type background fits nicely to the Ag3d and C1s CL spectra. This finding is consistent with the well-established rule that only Shirley background can be applied to the spectra obtained with high photon energy (e.g. 1486.6 eV).[21] The bottom spectra in both panels are the ones obtained after the Shirley background is subtracted. In all the spectra, as shown in Fig. 3, only the Shirley-type background is subtracted. Before going into a detailed explanation as to how the overlayer and substrate photoemission peaks intensities evolve with respect to molecular coverage, we would like to explain the method employed in coverage determination. After each deposition step followed by the Shirley background subtraction, the behavior of the FePc overlayer and Ag substrate intensities (C1s, Ag3d, respectively) can be well described by the exponential increase/decrease laws given in terms of the basic intensity Eqs. (1a) and (1b),[20]

$$\frac{I_{\mathrm{C}}^{\mathrm{d}}}{I_{\mathrm{C}}^{\infty}} = 1 - \exp\left(\frac{-d}{\lambda_{\mathrm{C}}\cos\theta}\right), \tag{1a}$$

$$\frac{I_{\mathrm{Ag}}^{\mathrm{d}}}{I_{\mathrm{Ag}}^{\infty}} = \exp\left(\frac{-d}{\lambda_{\mathrm{Ag}}\cos\theta},\right) \tag{1b}$$

Here: $d$ is overlayer coverage; $I_{\mathrm{C}}^{\mathrm{d}}$ and $I_{\mathrm{Ag}}^{\mathrm{d}}$ are the respective signal intensities (i.e. peak areas) from C1s and Ag3d states with an examined thickness; $I_{\mathrm{C}}^{\infty}$ and $I_{\mathrm{Ag}}^{\infty}$ are the intensities from the thick adsorbate (C1s) and bare substrate (Ag3d), in that order; $\lambda_{\mathrm{C}}$ and $\lambda_{\mathrm{Ag}}$ are the inelastic mean free paths (IMFP) of the C1s orbital of the adsorbate and Ag3d orbital of the substrate, respectively; $\theta$ accounts for the emission angle with respect to the surface normal, which in the present case is 78°. In order to obtain true overlayer thickness $d$, we separately determined the IMFPs of Ag3d and C1s levels by using Eqs. (2a) and (2b),[20]

$$\lambda_{\mathrm{Ag}} = \lambda = 538\,(E_{\mathrm{kin}})^{-2} + 0.41\,(a\cdot E_{\mathrm{kin}})^{0.5}, \tag{2a}$$

$$\lambda_{\mathrm{C}} = \lambda_{\mathrm{d}} = 49(E_{\mathrm{kin}})^{-2} + 0.11\,(a\cdot E_{\mathrm{kin}})^{0.5}, \tag{2b}$$

where $\lambda$ and $\lambda_{\mathrm{d}}$ are in units of monolayers and in mg·m$^{-2}$, respectively; $a$ (in nm) is extracted from $\rho N a^3 = M$ with the density ($\rho$) in kg/m$^3$; $N$ the Avogadro constant ($N = 6.02 \times 10^{23}$/mol)[22] and $M$ the atomic or molecular mass.[20] The kinetic energy ($E_{\mathrm{kin}}$) is expressed as $E_{\mathrm{kin}} = h\nu - E_{\mathrm{B}} - \phi_{\mathrm{spec}}$, where the last quantity is the work function of the spectrometer (4.6 eV). By taking into account $M_{\mathrm{FePc}}$ (568.37), $M_{\mathrm{Ag}}$ (107.88), $\rho_{\mathrm{Ag}}$ (10.5 kg/m$^3$),[23] $\rho_{\mathrm{FePc}}$ (1600 kg/m$^3$)[13] and

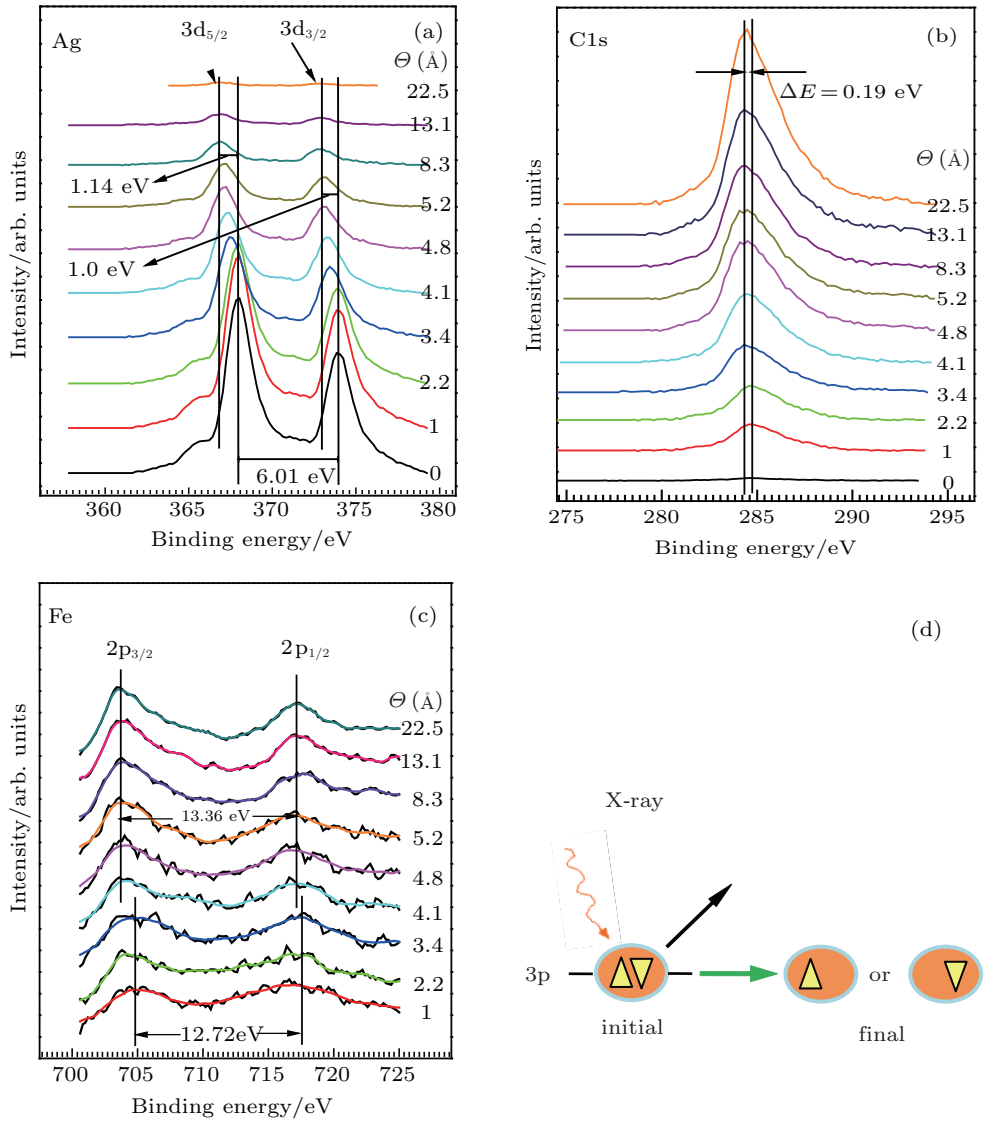



**Fig. 3.** (color online) MgK$_\alpha$ XP spectra for (a) Ag3d, (b) C1s, and (c) Fe2p core level as a function of FePc coverage on Ag (110) surface. (d) The initial and final states involved in the photoemission process. After electron emission from a 3p orbital subshell, the remaining election can have a spin-up or spin-down state. Magnetic interaction between these photoemitted electrons and the orbital angular momentum lead to spin–orbit coupling. On the basis of this process, Ag3d and Fe2p photoemission peaks split into two subpeaks.

corresponding core level $E_{\rm kin}$ energies (Table 1), and with the basic algebraic calculations, we estimated the overlayer and substrate mean free paths, i.e. $\lambda_{\rm C} = 25.9$ Å for the C1s line and $\lambda_{\rm Ag} = 15.3$ Å for the Ag3d line. Likewise, by using the molecular weight of Fe ($M_{\rm Fe} = 55.84$), density ($\rho_{\rm Fe} = 7.87$ kg/m$^3$),[23] and the respective $E_{\rm kin}$ of Fe2p, we obtained $\lambda_{\rm Fe} = 12.8$ Å.[24] The estimated values on one hand agree well with the previously determined values[25] and on the other hand coincide nicely with what is expected on the basis of the Seah and Dench universal curve.[20] All these values are summarized in Table 1.

**Table 1.** Values of the inelastic mean free paths ($\lambda_i$, Å) for different electron levels as extracted by using the above expressions. Experimental binding energy (Exper., $E_{\rm B}$) and calculated kinetic energy (Cal., $E_{\rm kin}$) are in eV.

| Electron level | Exper. $E_{\rm B}$ | Cal. $E_{\rm kin}$ | Meas. $\lambda_i$ | $\lambda_i$ Refs. [25] and [26] |
|---|---|---|---|---|
| Ag3d$_{5/2}$ | 367.8 | 1114.2 | 15.1 | 15.3, 15.6 |
| C1s | 284.47 | 1197.5 | 25.9 | 35.2, 26.2 |
| Fe2p$_{3/2}$ | 704.6 | 777.4 | 12.8 | 13.7 |

Fitting the experimental data with the above expressions yields nominal thicknesses of 1.0, 2.2, 3.4, 4.1, 4.8, 5.2, 8.3, 13.1, and 22.5 Å for the total deposition times of 60, 120, 180, 240, 300, 360, 420, 480, 540 s, respectively. The CL spectra acquired at increasing molecular coverage are shown in Fig. 3, panels (a)–(c), for the Ag3d, C1s, and Fe2p CL emissions, respectively. Spectra in each panel are normalized to the same height for better comparison. The bottom spectrum corresponds to the zero deposition time. The major substrate core levels (SCLs) Ag3d$_{3/2}$ and Ag3d$_{5/2}$ for the clean substrate are, respectively, at binding energies of 373.96 eV and 367.95 eV. The spectra for the silver substrate are exactly similar to what has been previously observed by our research group.[26] However, a small peak caused by the weak intensity X-ray emis-

sions is accompanied by the Ag3d peaks. This smaller peak exists with the spectrum because the X-ray emissions with weaker intensities were not subtracted from the data. Upon depositing FePc, the Ag3d and C1s peaks exhibit practically no shift, except for the decrease/increase in intensity, which indicates a weak interaction between the adsorbate and the substrate. This weak interaction was previously revealed for the case of $H_2Pc$ on InAs (100) and InSb (100) by synchrotron-based PES[14] and FePc on Ag (111) and Au (100) by photoexcited electron spectroscopies (CL-PES and VL-PES) and X-ray absorption spectroscopy (XAS).[15] The C1s and Fe2p PE originate from FePc molecules. Figure 3(b) shows that the C1s feature is located at 284.66 eV. Figure 3(c) indicates that $Fe2p_{1/2}$ and $Fe2p_{3/2}$ are located at 17.53 eV and 704.84 eV, respectively. These energies indicate that the overlayer signals are detectable at very low coverage, i.e., $\sim 1$ Å. Until the deposition time of 180 s, minimal changes in the shape of the features are observed.

With the sequential increase of film thickness, the intensities of C1s and Fe2p gradually increase while the intensity of Ag3d decreases. After 540 s of total deposition time (coverage $\sim 22.5$ Å), the C1s and Fe2p signals associated with FePc are fully developed and the Ag3d signal almost completely vanishes. Figure 3 further dictates that all the CL peaks shift towards lower binding energies, each by a different magnitude. The $Ag3d_{5/2}$ peak shifts by 1.14 eV while $Ag3d_{3/2}$ shifts by 1.0 eV. On the other hand $Fe2p_{3/2}$ shifts by 1.12 eV, and $Fe2p_{1/2}$ by 0.48 eV. In both cases the shift is towards the lower binding energy. The broadening and shifting of the Fe2p PE spectra towards lower binding energy suggests an increase of electron density at the Fe ion.[27] Also, the doublet separation between both the Ag3d and Fe2p CL spectra is increased but it is greater in the case of Fe2p than Ag3d, i.e., it increases from 6.01 eV to 6.15 eV for Ag3d and from 12.72 eV to 13.36 eV for Fe2p line. Figures 3(a) and 3(c) also follow the trend for the doublet separation, i.e., $p > d$.[22]

All the electron levels energies for the thin (1 Å) and thick films (22.5 Å), energy shifts ($\Delta E$), and the doublet separation (DS) are added in Table 2. Figure 3(b) and Table 2 reveal that in the case of the C1s electron level, neither a larger shift nor a significant change in the shape of the feature is observed. A greater change and larger shift in F2p PE as compared to the C1s emissions is observed, which indicates that the molecule–substrate interaction is mainly via the iron atom located at the center of the molecule. This observation strengthens the view that MPcs (especially FePc, CoPc) strongly interact with the metal substrates via the central metallic atom of the adsorbed molecule.[11–17,27] In contrast to this, FePc interacts weakly when adsorbed on a semiconducting substrate where the interaction is mainly through the Pc rings.[28] A critical analysis of the core level's shift on one hand indicates the modification of the electronic structure of the organic molecules, due to a greater interaction at the interface, and on the other hand it gives a sign of the charge transfer from the metallic substrate to the organic molecule. This supports the previously stated conclusions that an electronic charge transfers from Ag (110) to FePc[13,14,17] and from Au (110) to CoPc and FePc.[13,15] Thus, the metallic substrates (Ag, Au) and MPcs (FePc, CoPc) can be characterized as donor and acceptor materials, respectively. However, when FePc is adsorbed on $TiO_2$ (110) then it donates electronic charge to the semiconducting substrate, as revealed by the synchrotron-based PES and XAS.[29]

**Table 2.** All the core level binding energies, peak shifts ($\Delta E$), and doublet separation (DS) in photoelectron lines for the thin (1 Å) and thick (22.5 Å) coverage are in eV. A trend in the DS ($p > d$) is clearly visible.

| Electron level | Thin film | Thick film | $\Delta E$ | DS | |
|---|---|---|---|---|---|
| | | | | Thin film | Thick film |
| C1s | 284.66 | 284.47 | 0.19 | – | – |
| $Ag3d_{3/2}$ | 373.96 | 372.96 | 1.0 | 6.01 | 6.15 |
| $Ag3d_{5/2}$ | 367.95 | 366.81 | 1.14 | | |
| $Fe\ 2p_{1/2}$ | 717.53 | 717.05 | 0.48 | 12.72 | 13.36 |
| $Fe\ 2p_{3/2}$ | 704.81 | 703.69 | 1.12 | | |

This discussion then leaves us with very fundamental questions: what is the exact nature of FePc? (Is it a p-type or n-type semiconductor? Why does FePc deposited on different substrates behave so differently?) Figure 3(d) illustrates the initial and final states involved in the PE process. It discloses the secrets as to why Ag3d and Fe2p split into two components or subpeaks. A pair of electrons in a 3p orbital is schematically demonstrated, which tells that two energetically equivalent final states are possible — 'spin up' and 'spin down.' However, for an open shell [like Fe (in FePc) and Ag)] with two states of the same energy, a magnetic interaction between the spin of the electron (up or down) and its orbital angular momentum leads to spin–orbit coupling. This spin–orbit coupling, or equivalently $j$–$j$ coupling, ultimately leads to splitting of the Fe2p and Ag3d photoemitted lines into two components.[22] In order to shed more light on the C1s PE spectra we reconsider Fig. 3(b). The overall insufficient energy resolution of the CL-PES spectrometer (0.85 eV) prohibited us from observing PE from multiple sites within the organic molecule, as is observed in the cases of FePc on Ag (110),[14] CoPc on Ag (111),[27] FePc on TiO2,[29] $H_2Pc$ on compound semiconductors,[9] or FePc on HOPG;[30] however, our C1s CL spectra do resemble the one observed for NiPc on Au and Ag.[31]

Therefore, the C1s peak for the thickest organic overlayer (22.5 Å), also called the parent peak, is decomposed into chemically different species (benzene carbons–$C_{benz}$, pyrrole carbons–$C_{pyr}$, and their respective satellites (sa) ($C_{benz.sa}$, $C_{pyr.sa}$) as shown in Fig. 4. The molecular structure of FePc is added in the inset of Fig. 4. The binding energies of the C1s components attributed to the thickest organic overlayer are: 284.3 eV for $C_{benz}$, 285.6 eV for $C_{pyr}$, 286.22 eV for $C_{benz.sa}$, and 287.59 eV for $C_{pyr.sa}$. These values deviate slightly from

the C1s of NiPc grown on Au and Ag[31] but closely resemble those observed for FePc deposited on HOPG.[30] Apparently, the benzene: pyrrole intensity ratio appears close to the expected ratio (3:1), but in fact it varies slightly due to the shakeup process. Generally, the CL-PES of C1s peaks shows the same molecular features for both mono- and multilayer films. Therefore, only thick film is resolved into four components.

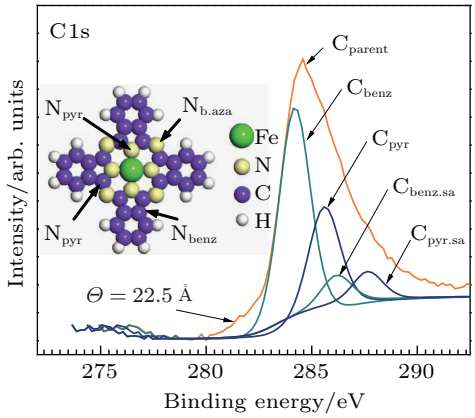



**Fig. 4.** (color online) Best fit of the C1s core level spectrum ($C_{parent}$) of bulk FePc. A schematic perspective view of an iron phthalocyanine (FePc: $C_{32}$ $H_{16}$ $N_8$ Fe) molecule is added in the inset. The peaks belonging to the benzene carbon ($C_{benz}$), pyrrole carbon ($C_{pyr}$) atoms and their respective satellites ($C_{benz.sa}$ and $C_{pyr.sa}$) are shown. Please see the text for detail.

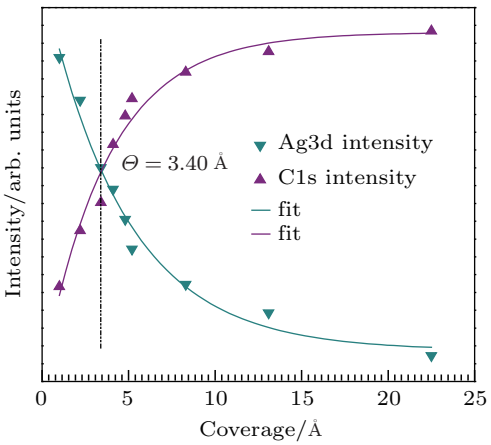



**Fig. 5.** (color online) Variation of C1s and Ag3d XPS signals as a function of FePc deposition. This so-called growth/decay curve is extracted from the intensities of the C1s and Ag3d core levels. Point-up and point-down triangular symbols correspond to C1s and Ag3d peak intensities, respectively.

Before ending the discussion, the intensities of the Ag3d and C1s peaks are compared during the formation of the interface, in order to get an understanding of the growth modes. Figure 5 demonstrates the underlying substrate and the overlayer photoemission peak intensities' evolution as a function of FePc coverage. The trends in the FePc–Ag (110) intensities for both the adsorbate and substrate are fitted very well with the two exponential fits. (Up-pointing triangular symbols are the exponential increase of C1s intensity, and down-pointing triangles are the exponential decrease of Ag3d intensity.) An exponential increase/decrease in the C1s/Ag3d signal is visible. Moreover, initially, the Ag3d emission is strongly suppressed while a large increase in the C1s intensity is measured. From the graph it appears that until the deposition time of 180 s, FePc adopts a Frank-van der Merwe (FM) growth mode, since until 3.40 Å coverage, the slopes of the over- and underlayer signals are almost uniform. Beyond the film thickness of $\sim 3.40$ Å, the slopes of both the core levels change leading to a change in growth mode, indicating that FePc on Ag (110) now follows Stranski–Krastanov (SK) growth mode. Thus from this figure, we can safely conclude that FePc thin films initially develop following the FM growth mode and then transform to SK mode, resulting in three-dimensional (3D) islands. This finding is consistent with Refs. [11], [15], and [17] but inconsistent with Ref. [32].

## 4. Conclusion

In conclusion, we have studied the proper coverage determination and the epitaxial growth mode of FePc on Ag (110) by X-ray photoelectron spectroscopy. All the core level spectra exhibited rigid shifts towards lower binding energies following the deposition of the organic films, each by a different magnitude. The doublet separation between $Fe2p_{3/2}$ and $Fe2p_{1/2}$ is increased from 12.72 eV to 13.36 eV for the thin and thick films, respectively. In addition to this, a greater shift in the Fe2p electron level as compared to C1s emission is observed, which indicates that the molecule–substrate interaction is chiefly via the iron atom located at the center of the organic molecule. An increase/decrease in the intensity of C1s/Ag3d is found to be exponentially linked to the overlayer molecular coverage. From the so-called growth/decay curve we conclude that FePc thin films initially develop following the FM growth mode and then transform to SK mode, resulting in 3D islands.

## References

[1] Ma J, Wang J and Liu Y 2007 *J. Power Sources* **172** 220
[2] Chen Y H and Lin B R 2011 *Cambridge J. Online* **46** 1270
[3] Heutz S, Mitra C, Wu W, Fisher A J, Kerridge A, Stoneham M, Harker T H, Gardener J, Tseng H H, Jones T S, Renner C and Aeppli G 2007 *Adv. Mater.* **19** 3618
[4] Naber W J M, Faez S and van der Wiel W G 2007 *J. Phys. D: Appl. Phys.* **40** 0022
[5] Moon H K, Son M, Park J F, Yoon S M, Lee S H and Choi H C 2012 *NPG Asia Materials* **4** 1
[6] Kroll T, Kraus R, Schönfelder R, Aristov V Yu, Molodtsova O V, Hoffmann P and Knupfer M 2012 *J. Chem. Phys.* **137** 054306
[7] Zhao A, Li Q, Chen L, Xiang H, Wang W, Pan S, Wang B, Xiao X, Yang J, Hou J G and Zhu Q 2005 *Science* **309** 1542
[8] Braun S, Salaneck W R and Fahlman M 2009 *Adv. Mater.* **21** 1450
[9] Palmgren P, Priya B R, Niraj N P P and Gothelid M 2006 *J. Phys.: Condens. Matter* **18** 10707
[10] Ahlund J, Schnadt J, Nilson K, Göthelid E, Schiessling J, Besenbacher F, Martensson N and Puglia C 2007 *Surf. Sci.* **601** 3661
[11] Casarin M, Marino M Di, Forrer D, Sambi M, Sedona F, Tondello E, Vittadini A, Barone V and Pavone M 2010 *J. Phys. Chem. C* **114** 2144
[12] Fortuna S, Gargiani P, Betti M G, Mariani C, Calzolari A, Modesti S and Fabris S 2012 *J. Phys. Chem. C* **116** 6251

[13] Betti M G, Gargiani P, Frisenda R, Biagi R, Cossaro A, Verdini A, Floreano L and Mariani C 2010 *J. Phys. Chem.* **114** 21638

[14] Palmgren P, Angot T, Nlebedim C I, Layet J M, Le Lay G and Göthelid M 2008 *J. Chem. Phys.* **128** 064702

[15] Petraki F, Peisert H, Aygu I U, Latteyer F, Uihlein J, Vollmer A and Chasse T 2012 *J. Phys. Chem. C* **116** 11110

[16] Takami T, Carrizales C and Hipps K W 2009 *Surf. Sci.* **603** 3201

[17] Qian H Q, Jiang L, Rehman A, Zhang H J, Li H Y, He P and Bao S N 2012 *Chem. Phys. Lett.* **537** 53

[18] Lin H C, Polaske N W, Oquendo L E, Gliboff M, Knesting K M, Nordlund D, Ginger D S, Ratcliff E L, Beam B M, Armstrong N R, McGrath D V and Savedra S S 2012 *J. Phys. Chem. Lett.* **3** 1154

[19] Lu B, Zhang H J, Li H Y, Bao S N and He P 2003 *Phys. Rev. B* **68** 125410

[20] Seah M P and Dench W A 1979 *Surf. Interf. Anal.* **1** 2

[21] Shirley D A 1972 *Phys. Rev. B* **5** 4709

[22] Vickerman J C and Gilmore I S 2009 *Surface Analysis — The Principal Techniques*, 2nd edn. (John Wiley and Sons, Ltd.)

[23] Rajput R K 2006 *Utilization of Electrical Power* (New Delhi Laxmi Publications Ltd.)

[24] Tanuma S, Powell C J and Penn D R 1991 *Surf. Interf. Anal.* **17** 911

[25] Jablonski A and Powell C J 1999 *J. Electron Spectr. Relat. Phenom.* **100** 137

[26] Wu H F, Zhang H J, Lu Y H, Si J X, Li H Y, Bao S N, Wu H Z and He P 2008 *Appl. Phys. Lett.* **92** 122112

[27] Schmid M, Kaftan A, Steinrück H P and Gottfried J M 2012 *Surf. Sci.* **606** 945

[28] Rehman R A, Zhang H J, Qian H Q, Dan J, Dou W D, Li H Y, He P and Bao S N 2012 *Physica E* **44** 1572

[29] Palmgren P, Nilson K, Yu S, Hennies F, Angot T, Nlebedim C I, Layet J M, Lay G L and Gothelid M 2008 *J. Phys. Chem. C* **112** 5972

[30] Isvoranu C, Åhlund J, Wang B, Ataman E, Mårtensson N, Puglia C, Andersen J N, Bocquet M L and Schnadt J 2009 *J. Chem. Phys.* **131** 214709

[31] Petraki F, Papaefthimiou V and Kennou S 2007 *Org. Electron.* **8** 522

[32] Ellis T S, Park K T, Ulrich M D, Hulbert S L and Rowe J E 2006 *J. Appl. Phys.* **100** 093515